Fabrication Flaws in Reactor Pressure Vessel Repair Welds

George J. Schuster and Steven R. Doctor

Pacific Northwest National Laboratory[a], Richland, WA

ABSTRACT

The Pacific Northwest National Laboratory (PNNL) is developing a generalized flaw size and density distribution for the population of U.S. reactor pressure vessels (RPVs). The purpose of the generalized flaw distribution is to predict vessel-specific flaw rates for use in probabilistic fracture mechanics calculations that estimate vessel failure probability. Considerable progress has been made on construction of an engineering database of fabrication flaws in U.S. nuclear RPVs. The fabrication processes and product forms used to construct U.S. RPVs are represented in the database.

This paper describes the fabrication flaw distribution and characterization in the repair weld metal of reactor pressure vessels. This work indicates that large flaws occur in these repairs and the flaws are complex in composition and sometimes include cracks on the repair ends. Parametric analysis using an exponential fit is performed on the data. A description of repair flaw morphology is provided. Fabrication flaws in repairs are: characterized using high-sensitivity nondestructive ultrasonic testing, validated by other nondestructive evaluation (NDE) techniques, and complemented by destructive testing.

INTRODUCTION

The U.S. Nuclear Regulatory Commission (NRC) initiated a program at PNNL with the major objective of estimating the rate of occurrence of fabrication flaws in U.S. light-water reactor pressure vessels and piping welds [1]. PNNL's methodology for estimating the density and size distribution of fabrication flaws involves the NDE of weldments from cancelled nuclear plants and the destructive validation of detected flaws. This methodology characterizes the flaws for fracture mechanics significance because the likelihood of vessel failure is sensitive to flaw location, type, size, orientation, and other flaw characterizations [2]. The objective of this research is to estimate these and other relevant properties of flaws created during the fabrication of nuclear component weldments.

To meet this objective, a generalized flaw distribution is proposed because the rate of occurrence of fabrication flaws is expected to vary over product forms and over the years of component fabrication. In order to develop a generalized flaw distribution and to resolve technical issues, an expert judgment process was used. The results of this expert judgment process helped to formulate a generalized approach to fabrication flaw density and distribution [3]. The impaneled experts judged that the product forms and construction processes determine the fabrication flaws in weldments. So, for the *i*th component, the number of flaws greater than size x, $N_i(x)$, can be given by a sum over product forms

$$N_i(x) = \sum_j \rho_j(t_i) \cdot V_{ij} \cdot G_j(x) \tag{1}$$

where $\rho_j(t)_i$ is the flaw density in product form j during time interval for the construction of the *i*th component t_i, V_{ij} is the volume (or area) of the product form in a weldment or a region of a weldment, and $G_j(x)$ is the probability that a flaw, in product form j, has a size greater than x. PNNL data have shown that

$$G_j(x) = exp(-\beta_j x) \tag{2}$$

provides a reasonable fit to the fabrication flaw data [4].

[a] The work was sponsored by the U.S. Nuclear Regulatory Commission under Contract DE-AC05-76RL01830; NRC JCN Y6604; Wallace E Norris, NRC Project Monitor.

MEASUREMENT AND APPARATUS

Because it is an important part and key step of the measurement process for fabrication flaw density and distribution, this section discusses the implementation and application of ultrasonic imaging for sub-wavelength resolution on clusters of fabrication flaws. Work on the Synthetic Aperture Focusing Technique (SAFT) algorithm is reported that produced an improvement of three orders of magnitude in processing times. High-resolution reconstructions that previously took more than a day can now be completed in under a minute. This paper shows how SAFT-UT images can now resolve closely spaced small flaws and more accurately size them as well. Ultrasonic imaging systems that can distinguish two objects that are separated by less than a wavelength of the ultrasound can provide high-resolution images. SAFT systems have been proposed for this purpose over the years [5].

In the past it was argued that SAFT can provide the needed imaging for characterizing flaws in reactor pressure vessels. Generating images with sub-wavelength resolution for the vessel thickness has been the objective. The lateral resolution of a SAFT system is determined by the maxima of two separate resolution elements—the transducer's and the synthetic aperture's. In most ultrasonic applications of synthetic aperture focusing, the system resolution will be no better than the resolving power of the transducer that is used [6]. In field applications of synthetic aperture focusing for NDE of welded assemblies, flat elements are used for reasons of mechanical simplicity that arise from having the element contact and follow the metal surface. For flat elements, the lateral spatial resolution is just half the diameter of the element [7] and is independent of wavelength. Small contact probes, used in synthetic aperture focusing applications, typically have a 6-mm diameter that limits the system resolution to 3 mm.

Field inspections conducted with industrial systems generally use flat ultrasonic elements. In the laboratory, the use of spherical (focused) elements in ultrasonic imaging systems is widespread. For spherical elements, the transducer lateral resolution, ΔX_t, is given by

$$\Delta X_t = 1.22 \lambda_c f_L / A_t \tag{3}$$

where λ_c is the wavelength in the coupling material, f_L is the focal length of the transducer, A_t is the transducer aperture, and the factor of 1.22 comes from the first zero crossing of a Bessel function [8].

Synthetic aperture focusing permits the synthetic lens size to be chosen after the data are taken. For data processing, it is usually the intent to produce an image with shift-invariant resolution. To do this, the lens diameter is allowed to increase linearly with depth during data processing. The synthetic aperture angle, θ, describes this increasing lens diameter, and the synthetic aperture lateral resolution, ΔX_s, is given by

$$\Delta X_s = \lambda_m / 4 \tan \theta \tag{4}$$

where λ_m = wavelength in the metal.

Fig. 1 is a graph of the theoretical lateral resolution for images of reflectors in carbon steel. The graph shows the synthetic aperture resolution, using Eq. (3), and probe resolution, using Eq. (4), plotted against the aperture angle and how the resolution can approach the diffraction limit of half a wavelength.

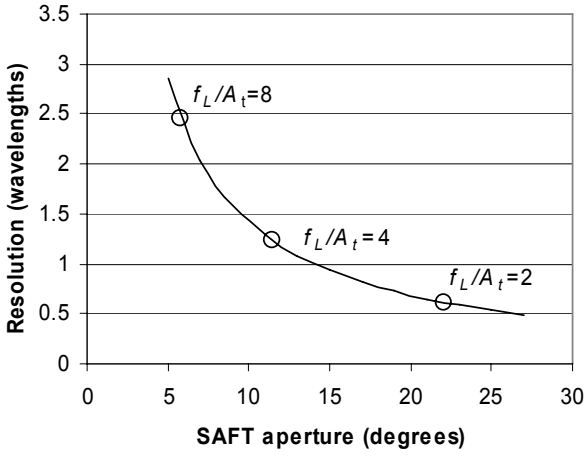

Fig. 1 Lateral Resolution in Wavelengths

The computational complexity of the SAFT reconstruction has limited its application in the field. Initial progress with the SAFT algorithm involved lookup tables that were calculated before the focusing of inspection volume started so that it eliminated the unnecessary repeating calculation of temporal shifts [9]. In that work, the inner loop of the SAFT algorithm used a list of off-center sample positions in the synthetic aperture to fetch the temporal shift and accumulate ultrasonic responses.

In Table 1, the first row reports the time to process the file, 36 hours, for the "by aperture list" algorithm. This is the computing solution where the inner loop of the SAFT algorithm used a list of off-center sample positions in the synthetic aperture to fetch the temporal shift and accumulate ultrasonic responses. For more information on the "By Aperture List" algorithm, see [9]. The focusing to achieve the 0.5-mm resolution required that 82,000 summations be performed per volume element (voxel) and the file had 1 million voxels.

Table 1. Some Focusing Times for SAFT Resolutions

Algorithm	Lens sampling (percent)	Time (hr:min:sec)	Sums per Voxel	Noise (counts)	Signal (counts)
By Aperture List	100	36:00:00	81729	23	725
By Cross Section	100	21:01	81729	23	743
By Cross Section	25	6:21	20432	41	739
By Cross Section	11	3:21	8990	58	769
By Cross Section	6	2:13	4904	78	694
By Cross Section	4	1:34	3269	96	714
By Cross Section	3	1:13	2452	116	767
By Cross Section	2	0:59	1635	127	712

The second line in Table 1 reports the results from a modified SAFT algorithm that completed the processing in 21 minutes, which is a factor of 100 improvement over "By Aperture List." The high-performance solution to the SAFT problem is obtained by minimizing the address change in the data to achieve the focusing [10]. Instead of focusing a voxel to completion, a vector of accumulators, $\vec{s}$, can be used to sum vectors of coherent ultrasonic responses

$$\vec{s'} = \vec{s} + \overrightarrow{r^c} \tag{5}$$

The vector equation forms the inner loop of the computation and the address change is 8 bytes if 32-bit integers are used. A cross section of accumulators can be used, in a similar fashion, while keeping the address change to a minimum. The solution, "By Cross Section", is fully described in [10].

Lens sampling can be used to achieve another factor of 10 or more improvement in processing time. In lens sampling, every n-1 summations are skipped in both lateral directions. So if n is set to 2, every other summation is skipped in both directions and only 25% of the summations are performed. The case of 25% lens sampling is shown on the third line in Table 1. A 2% lens sampling finishes the test calculation in about 1 minute. It should be noted that the 6 dB drop size of the 1-mm flat bottom hole remained the same for all of the cases reported in the table – 1 mm. Of course, the average signal, about 700 counts, does not change as the sampling percentage changes because the average is performed over the same lens size. Fig. 2 shows the signal-to-noise dependency on sums per voxel using the lens sampling algorithm described above. The dependency is fit with a power law function and the power is approximately the square root of the sums per voxel as expected.

Sizing performance can be seen in Fig. 3 for dual F2.8 (18-mm diameter and 50-mm focal length) transducers at 10 MHz operating in a pitch/catch mode. The steel test piece contained 1-mm to 8-mm diameter flat bottom holes. The results shown in Fig. 3 required 10^5 summations per volume element. The open circles, labeled contact, are results from using a 6-mm-diameter flat transducer. The error bars represent the 0.25-mm step size used for data acquisition.

RESOLVING CLUSTERS OF FABRICATION FLAWS

This section describes the results of high-resolution ultrasonic imaging on clusters of small fabrication flaws. The methods described in the previous section were applied and closely spaced small flaws were resolved in the focused images. The ultrasonic results were validated using metallography.

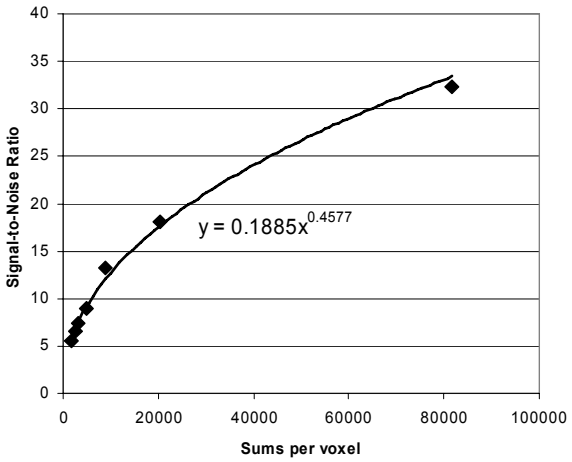

Fig. 2 Signal-to-Noise and Various Synthetic Lens Sampling

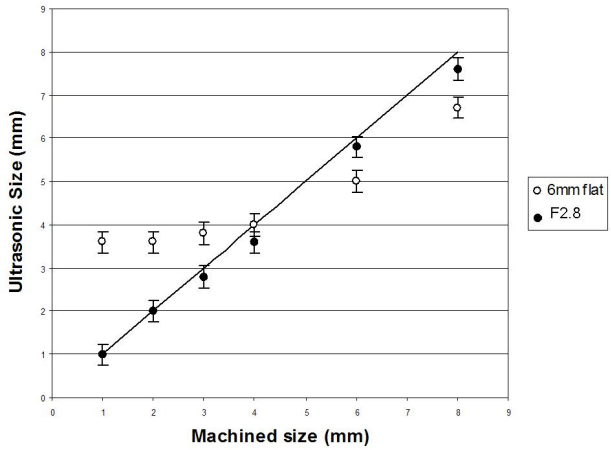

Fig. 3 Chart of Sizing Performance

On the left in Fig. 4 the immersion testing data of a 6-mm flaw indication from a weld-normal testing of a large weld segments is shown. The data that are shown here used a 10-MHz F8 immersion transducer with a lateral resolution of 2.5 wavelength or 1.5 mm. At this resolution the indication appears to be one flaw. Fig. 4, on the right, shows immersion testing data of the same 6-mm flaw indication as on the left. The data here used a 10-MHz F2.7 immersion transducer with a lateral resolution of 0.8 wavelength or 0.5 mm. In this image multiple, small 1-mm flaws are resolved. Fig. 5 shows one optical metallograph from the grinding, polishing, and etching of sample. The figure shows three small voids. Other voids were found in the grinding steps and the collection of these voids created the cluster image shown on the left in Fig. 4.

FABRICATION FLAWS IN REPAIRS

The complex shape and form of repair flaws are discussed in this section. The location of the flaws is provided with a description of their composition.

The largest repair flaw found in a seam weld of the Pressure Vessel Research User Facility (PVRUF) reactor pressure vessel had a through-wall dimension of 17 mm. This PVRUF 17-mm flaw was in a repair to the beltline weld of the PVRUF reactor pressure vessel. The repair was made from the outside diameter (OD) of the vessel to a depth of 16.5 cm. The flaw continued for three weld passes. At the end of the third weld pass, the flaw changed from side-wall lack of fusion to inter-run lack of fusion (between the repair metal weld passes). Fig. 6 is a micrograph of a portion of the PVURF 17-mm flaw. The location of this portion of the PVRUF 17-mm flaw is in the fusion zone of the repair metal. The composition of the flaw is slag, porosity, and contamination. Fig. 6 also shows a micrograph showing a magnified view of a portion of the PVRUF 17-mm flaw. A crack-like discontinuity is visible. The crack originates from a small contaminated region between the weld beads.

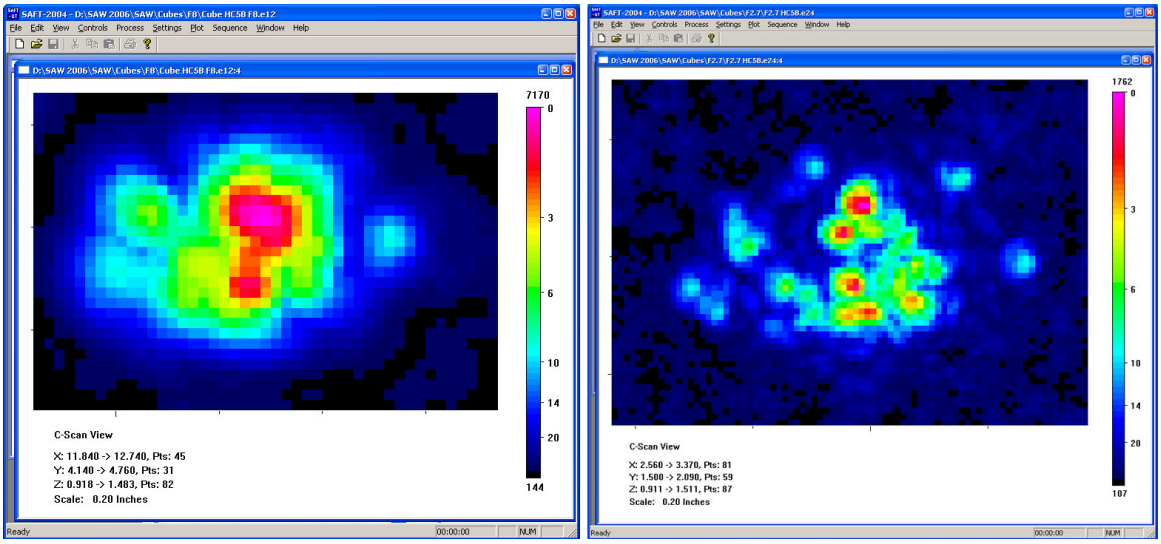

Fig. 4 SAFT-UT Images of Fabrication Flaw at Two Different Resolutions – F8 (2.5 mm resolution) on left and F2.8 (0.8 mm resolution) on right

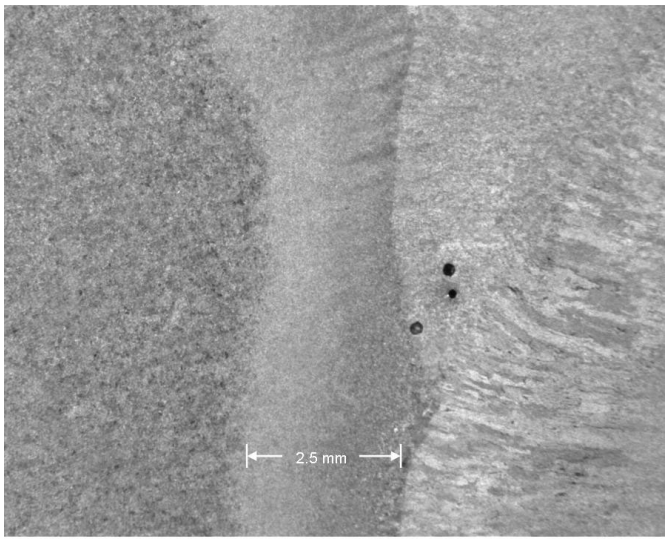

Fig. 5 Metallograph of Cluster of Small Voids Near the Fusion Line of the Base Metal with the Machine-Made Weld

Fabrication cracks are typically one of two general kinds. Cold cracking, also called heat-affected zone cracking, occurs during cooling when the stress of solidification causes the weaker solid metal adjacent to a weld bead to crack. The second type is hot cracking. A weld solidification crack is a type of hot crack that occurs in the weld metal of various alloys. It is not a problem except in cases in which the welding process is improperly controlled. Yet the occurrence of such cracks can greatly reduce the strength and integrity of welded components and is one of the serious problems in the welding of high-strength steels [11].

Hot cracking takes place as a result of the strains set up during the welding and occurs in thin films of nonmetallic segregates or by segregation of alloy elements, both of which lead to intergranular surfaces that solidify after the rest of the weld metal. Propagation of weld solidification cracks from weld pass to weld pass is described in [12]. Solidification cracking is intergranular and propagates due to the thermal stresses and contamination acting behind the solidifying pool.

Hot cracking, which includes weld solidification cracks, is intergranular and winding, and can occur as multiple cracks [13]. The most common orientation is cracking parallel to the weld direction, and the cracks can be located in the weld center. Hot cracks may occur in directions parallel to the solidification direction of the weld metal. An example of hot cracking in austenitic stainless steel weld metal is shown in [13].

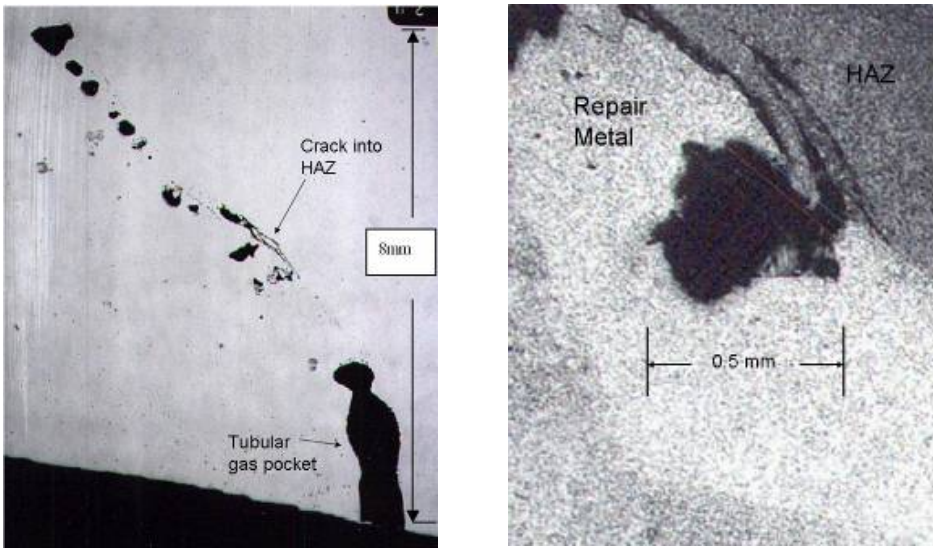

Fig. 6 Metallographs of Complex Repair Flaw Showing a Crack into the Heat Affected Zone

Lack of fusion is a weld discontinuity that is oriented along the fusion line of the weld with the base metal [13,14]. These discontinuities also occur between the weld passes. Lack of fusion is characterized in the literature as narrow, making it distinct from slag inclusions, which are round. Lack of fusion is also characterized as unbranched so as to be distinct from cracks. Lack of fusion can be oxide-filled.

Fig. 7 is a micrograph, as polished and etched, of a portion of the crack in the canceled nuclear power plant Hope Creek 2 RPV Specimen C2CC. This electron image shows the location, inside the crack, of the measurement of the elemental composition of the contamination in the crack. Fig. 7 also gives the elemental composition of contamination in the crack in Hope Creek 2 RPV Specimen C2CC; Fig. 8 provides the x-ray spectrum from that elemental analysis.

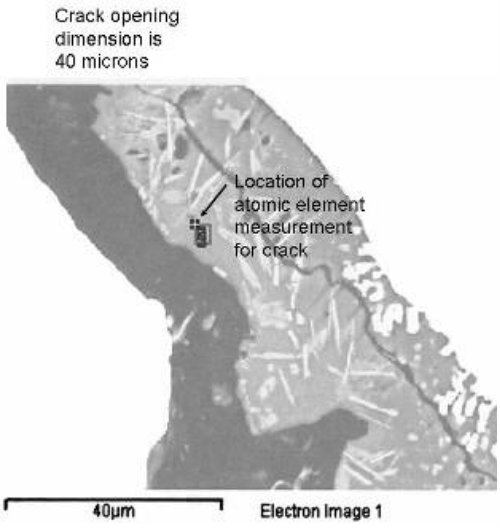

Standard :
O SiO2 28-Jan-2004 05:14 PM
Na Albite 1-Jun-1999 12:00 AM
Mg MgO 1-Jun-1999 12:00 AM
Al Al2O3 1-Jun-1999 12:00 AM
Si SiO2 28-Jan-2004 05:15 PM
S FeS2 1-Jun-1999 12:00 AM
K MAD-10 Feldspar 1-Jun-1999 12:00 AM
Ca Wollastonite 1-Jun-1999 12:00 AM
Ti Ti 1-Jun-1999 12:00 AM
Mn Mn 1-Jun-1999 12:00 AM
Fe Fe 1-Jun-1999 12:00 AM

Element	App Conc.	Intensity Corrn.	Weight %	Weight % Sigma	Atomic %
O K	24.65	0.6217	38.36	1.03	60.16
Na K	0.84	0.6088	1.33	0.15	1.45
Mg K	0.35	0.5963	0.57	0.10	0.59
Al K	0.58	0.7217	0.78	0.10	0.72
Si K	12.94	0.8428	14.85	0.32	13.27
S K	0.20	0.8550	0.23	0.08	0.18
K K	12.55	1.0883	11.15	0.26	7.16
Ca K	8.31	0.9826	8.18	0.22	5.12
Ti K	2.42	0.8345	2.80	0.15	1.47
Mn K	12.47	0.8325	14.48	0.37	6.62
Fe K	6.42	0.8547	7.26	0.29	3.26
Totals			100.00		

Fig. 7 Electron Image and Elemental Analysis of Crack in a Fabrication Flaw in a Weld Repair

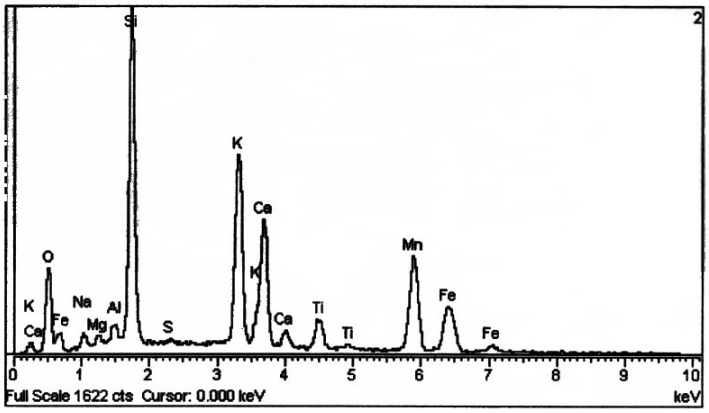

Fig. 8 Spectrograph from the Elemental Analysis shown in Fig. 7

DISTRIBUTION OF REPAIR FLAWS

PNNL's laboratory data acquired on repairs in weld segments were analyzed to determine the fabrication flaw density and size distribution. Weld segments from three reactor pressure vessels and one dissimilar metal weld piping section were found to contain weld repairs. The NDE inspections detected many fabrication flaws in the repairs, and the data were analyzed for density and distribution. An estimate of flaw density and distribution was made for five cases.

The results for the through-wall size distribution are given in Fig. 9. The through-wall dimensions of repair flaws span a range extending from 2 mm to 17 mm. For the five flaw distributions shown in Fig. 9, significant differences can be seen—a factor of 10 difference in some cases. The distributions of flaws for the seam weld repairs from three vessels (the PVRUF, Shoreham, and Hope Creek Unit 2 repairs) should have similar slopes; the variability can be attributed to the small number of repairs examined. The fabrication flaw density and distribution in repair metal does not appear to depend on vessel vintage. In Fig. 9, the distribution of flaws for weld preparation surface repairs is shown to be higher than that of flaws in weld seam repairs. This is to be expected because the repair metal in this case contacts the mid-wall segregates in the base metal. The distribution of flaws in the repairs found in the three piping repairs spans a limited range, from 2 mm to 4 mm.

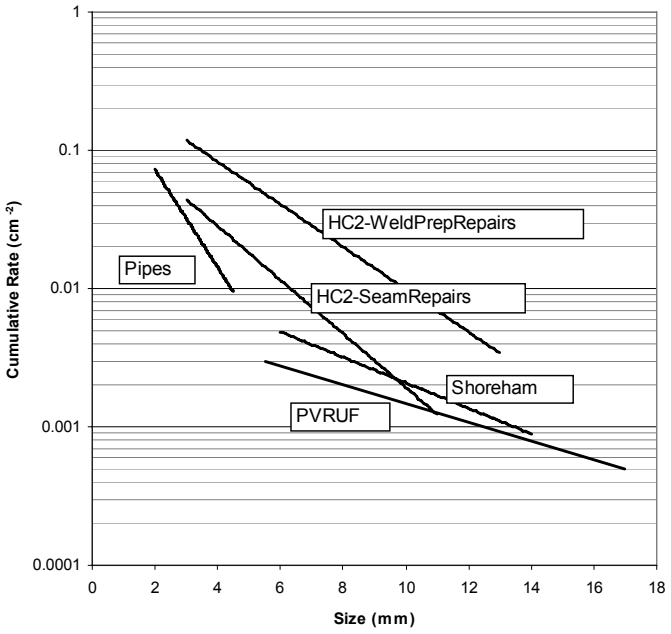

Fig. 9 Comparison of Flaw Density and Through-wall Size Distribution for Repair Flaws in Three Reactor Pressure Vessels and in Dissimilar Metal Welds of Piping

SUMMARY AND CONCLUSIONS

A generalized flaw distribution was presented that parameterizes the rate of occurrence of fabrication flaws with respect to product forms and the years of component fabrication. An expert judgment process was used in order to develop the generalized flaw distribution. The impaneled experts judged that the product forms and construction processes determine the fabrication flaws in weldments.

Part of the measurement process for fabrication flaw density and distribution used an implementation and application of ultrasonic imaging for sub-wavelength resolution on clusters of fabrication flaws. Work on the Synthetic Aperture Focusing Technique (SAFT) algorithm was reported that produced an improvement of three orders of magnitude in processing times. High-resolution reconstructions that previously took more than a day can now be completed in under a minute. This paper shows how SAFT-UT images can now resolve closely spaced small flaws and more accurately size them as well.

An example of high resolution ultrasonic imaging of a cluster of fabrication flaws was provided. At low resolution the ultrasonic indication appeared to be one flaw. High resolution ultrasonic data with a lateral resolution of 0.8 wavelength was provided. In this image multiple, small 1-mm flaws are resolved.

The repair flaws were found to be complex. Metallographic analysis of repair flaw specimens shows that the fabrication flaws are composed of a mixture of cracks, lack of fusion, contamination, and porosity. The repair flaws can repeat on the next weld pass. This phenomenon is of known interest to the modeling of welding flaws. Distributions were developed for flaws in repairs in various RPV product forms that showed significantly different densities.

REFERENCES

1. Jackson, D.A., Doctor, S.R., Schuster, G.J. and Simonen, F.A., "Developing a generalized flaw distribution for reactor pressure vessels," *Nuclear Engineering and Design*, Vol. 208, 2001, pp. 123-131.
2. Simonen, F.A. and Khaleel, M.A., "A Model for Predicting Vessel Failure Probabilities Due to Fatigue Crack Growth," *Pressure Vessel and Piping Conference Fatigue and Fracture Mechanics*, Vol. PVP Vol. 304, pp. 401-416, 1995.
3. Jackson, D.A. and Abramson, L., *Report on the Preliminary Results of the Expert Judgment Process for the Development of a Methodology for a Generalized Flaw Size and Distribution for Domestic Reactor Pressure Vessels*, MEB-00-01, PRAB-00-01, U.S. Nuclear Regulatory Commission, Washington, DC, 2000.
4. Doctor, S.R. and Schuster, G.J., Destructive Validation Methodology and Results for the Characterization of Flaws in Nuclear Reactor Pressure Vessels, *3rd International Conference of NDE in Relation to Structural Integrity for Nuclear and Pressurized Components*, Seville, Spain, 2001.
5. Frederick, J.R., Vanden Broek, C., Ganapathy, S., Elzinga, M., De Vries, W., Papworth, D. and Hamano, N., *Improved Ultrasonic Nondestructive Testing of Pressure Vessels*, NUREG/CR-0909, U.S. Nuclear Regulatory Commission, Washington, DC, 1979.
6. Busse, L.J., Collins, H.D. and Doctor, S.R., *Review and Discussion of the Development of Synthetic Aperture Focusing Technique for Ultrasonic Testing, SAFT UT*, NUREG/CR-3625, PNL-4957, U.S. Nuclear Regulatory Commission, Washington, DC, 1984.
7. Schmitz, V., "Nondestructive Acoustic Imaging Techniques, Imaging of Complex Media with Acoustic and Seismic Waves," *Topics in Applied Physics*, Vol. 84, 2002, pp. 167-189.
8. Goodman, J.W., *Introduction to Fourier Optics*, McGraw-Hill, 1996.
9. Ganapathy, S., Schmult, B., Su, W.S., Hamano, N. and Bristor, D., *Investigation of Special Purpose Processors for Real-Time Synthetic Aperture Focusing Techniques for Nondestructive Evaluation of Nuclear Reactor Vessels and Piping Components*, NUREG/CR-2703, U.S. Nuclear Regulatory Commission, Washington, DC, 1983.
10. Schuster, G.J., Doctor, S.R. and Bond, L.J., "A System for High-Resolution, Nondestructive, Ultrasonic Imaging of Weld Grains," *IEEE Transactions on Instrumentation and Measurement*, Vol. 53, 2004, pp. 1526-1532.
11. Morgan-Warren, E.J. and Jordan, M.F., "A Quantitative Study of the Effect of Composition on Weld Solidification Cracking in Low-Alloy Steels," *Metals Technology*, Vol. 1, 1974, pp. 271-278.
12. Kou, S. and Le, Y., "Alternating Grain Orientation and Weld Solidification Cracking," *Metallurgical Transactions A*, Vol. 16A, 1985, pp. 1887-1896.
13. Ekstrom, P. and Wale, J., *Crack Characterization for In-service Inspection Planning*, SKI Report 95:70, Swedish Nuclear Power Inspectorate, Stockholm, Sweden, 1995.
14. Thielsch, H., *Defects and Failures in Pressure Vessels and Piping*, Reinhold Publishing Corp., New York, 1965.
15. Chapman, O.J.V. and Simonen, F.A., *RR-PRODIGAL – A Model for Estimating the Probabilities of Defects in Reactor Pressure Vessel Welds*, NUREG/CR-5505, PNNL-11898, U.S. Nuclear Regulatory Commission, Washington, DC, 1998.